

Two-step electronic response to magnetic ordering in a van der Waals ferromagnet

Han Wu¹,¹ Jian-Xin Zhu,^{2,3} Lebing Chen,^{4,1} Matthew W. Butcher¹, Ziqin Yue^{1,5}, Dongsheng Yuan^{6,7}, Yu He,⁸ Ji Seop Oh,^{1,4} Bin Gao,¹ Jianwei Huang,¹ Shan Wu,⁴ Cheng Gong,⁹ Yucheng Guo,¹ Sung-Kwan Mo,¹⁰ Jonathan Denlinger,¹⁰ Donghui Lu,¹¹ Makoto Hashimoto,¹¹ Matthew B. Stone,¹² Alexander I. Kolesnikov¹², Songxue Chi¹², Junichiro Kono,^{13,14,1,15} Andriy H. Nevidomskyy,¹ Robert J. Birgeneau^{1,4,6,16}, Pengcheng Dai,¹ and Ming Yi^{1,*}

¹*Department of Physics and Astronomy and Rice Center for Quantum Materials, Rice University, Houston, Texas 77005, USA*

²*Theoretical Division, Los Alamos National Laboratory, Los Alamos, New Mexico 87545, USA*

³*Center for Integrated Nanotechnologies, Los Alamos National Laboratory, Los Alamos, New Mexico 87545, USA*

⁴*Department of Physics, University of California at Berkeley, Berkeley, California 94720, USA*

⁵*Applied Physics Graduate Program, Smalley-Curl Institute, Rice University, Houston, Texas 77005, USA*

⁶*Materials Sciences Division, Lawrence Berkeley National Laboratory, Berkeley, California 94720, USA*

⁷*National Institute for Materials Science, 1-1 Namiki, Tsukuba, Ibaraki 305-0044, Japan*

⁸*Department of Applied Physics, Yale University, New Haven, Connecticut 06511, USA*

⁹*Department of Electrical and Computer Engineering and Quantum Technology Center, University of Maryland, College Park, Maryland 20742, USA*

¹⁰*Advanced Light Source, Lawrence Berkeley National Laboratory, Berkeley, California 94720, USA*

¹¹*Stanford Synchrotron Radiation Lightsource, SLAC National Accelerator Laboratory, Menlo Park, California 94025, USA*

¹²*Neutron Scattering Division, Oak Ridge National Laboratory, Oak Ridge, Tennessee 37831, USA*

¹³*Department of Electrical and Computer Engineering, Rice University, Houston, Texas 77005, USA*

¹⁴*Smalley-Curl Institute, Rice University, Houston, Texas 77005, USA*

¹⁵*Department of Material Science and Nanoengineering, Rice University, Houston, Texas 77005, USA*

¹⁶*Department of Materials Science and Engineering, University of California, Berkeley, California 94720, USA*

 (Received 7 June 2023; revised 9 November 2023; accepted 18 December 2023; published 12 January 2024)

The two-dimensional material $\text{Cr}_2\text{Ge}_2\text{Te}_6$ is a member of the class of insulating van der Waals (vdW) magnets. Here, using high resolution angle-resolved photoemission spectroscopy in a detailed temperature dependence study, we identify a clear response of the electronic structure to a dimensional crossover in the form of two distinct temperature scales marking onsets of modifications in the electronic structure. Specifically, we observe Te p -orbital-dominated bands to undergo changes at the Curie transition temperature T_C while the Cr d -orbital-dominated bands begin evolving at a higher temperature scale. Combined with neutron scattering, density functional theory calculations, and Monte Carlo simulations, we find that the electronic system can be consistently understood to respond sequentially to the distinct temperatures at which in-plane and out-of-plane spin correlations exceed a characteristic length scale. Our findings reveal the sensitivity of the orbital-selective electronic structure for probing the dynamical evolution of local moment correlations in vdW insulating magnets.

DOI: [10.1103/PhysRevB.109.045416](https://doi.org/10.1103/PhysRevB.109.045416)

Exploring the magnetism in quasi-two-dimensional (2D) materials has been a fascinating subject in quantum physics for more than five decades. This field has received strong stimuli from both the discovery of high temperature superconductivity in the lamellar copper oxides in the late 1980s and, more recently, studies of the ferromagnetism in van der Waals (vdW) materials [1–10]. The chromium tellurides $\text{Cr}_2\text{X}_2\text{Te}_6$ ($X=\text{Ge}$, Si , and Sn) belong to a category of insulators with intrinsic long-range ferromagnetic (FM) order down to the 2D regime [3,4,7,9–26]. $\text{Cr}_2\text{Ge}_2\text{Te}_6$, in particular, exhibits ferromagnetism with a T_C that ranges from 65 K in bulk to around 40 K when exfoliated down to bilayer flakes, with the easy axis along the c direction [27–33]. The nature of the magnetism in two dimensions in the vdW magnets can

be understood to originate from the magnetic anisotropy that can counteract the strong thermal fluctuations. A neutron scattering study on $\text{Cr}_2\text{Si}_2\text{Te}_6$ ($T_C = 35$ K) has provided direct evidence on the development of the magnetic order, where the exchange interaction along the c direction is much smaller than that in the in-plane directions, and the dynamic correlations can persist in the ab plane up to at least 300 K [34]. Such an effective three-dimensional (3D) to 2D crossover behavior of the magnetic order in $\text{Cr}_2\text{Si}_2\text{Te}_6$ has also been confirmed by spin correlation driven lattice distortions [35]. Electronically, these Cr-based vdW ferromagnets are gapped at the Fermi level due to strong Coulomb repulsion [23,25,36]. In contrast to the metallic Fe_nGeTe_2 ($n = 3-5$) systems, $\text{Cr}_2\text{Ge}_2\text{Te}_6$ as an insulating magnet with a simple magnetic order untangled with other competing or intertwined electronic orders is an ideal platform to study the impact of low dimensional magnetism on the electronic degree of freedom [26,37,38].

*mingyi@rice.edu

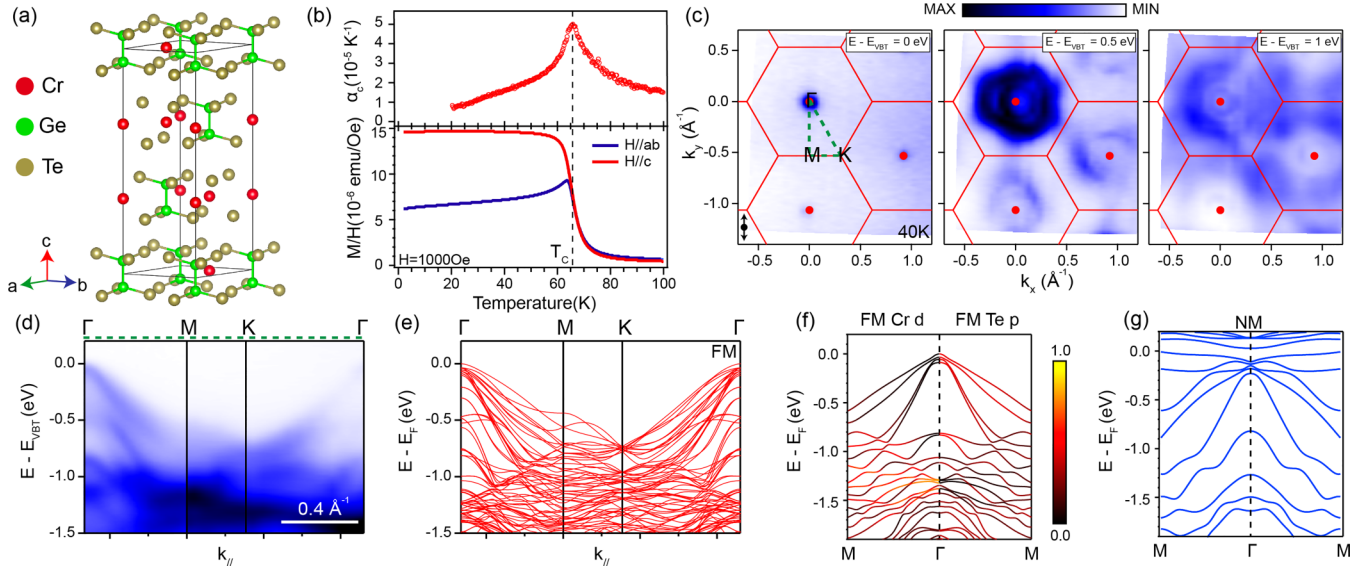


FIG. 1. Crystal structure, magnetization, and electronic structure of $\text{Cr}_2\text{Ge}_2\text{Te}_6$. (a) Crystal structure. (b) Dilatometry measurement of the c -axis thermal coefficient α (upper) and magnetization (lower). (c) ARPES constant energy contours measured in the FM phase at 40 K, with energy referenced to the valence band top. Brillouin zone centers and boundaries are shown, along with the polarization vector. (d) Spectral image along Γ - M - K - Γ as marked in (c). (e) DFT ferromagnetic calculation along Γ - M - K - Γ . (f) DFT calculated band structures of the ferromagnetic $\text{Cr}_2\text{Ge}_2\text{Te}_6$ projected onto the Cr- d and Te- p orbitals. (g) DFT calculations for the nonmagnetic state without local moments.

Here we report the observation of the electronic response to the development of the spin correlations across a wide range of temperatures in the vdW magnet $\text{Cr}_2\text{Ge}_2\text{Te}_6$ via angle-resolved photoemission spectroscopy (ARPES). By mapping out the temperature-dependent band structure and the one-electron spectral evolution across T_C , we observe two types of band evolutions: one group associated with Cr d orbitals that exhibits a gradual shift with an onset temperature well above T_C , and another associated with Te p orbitals that rapidly shift near T_C . From a combination of neutron scattering, Monte Carlo simulations, and density functional theory (DFT) calculations, we arrive at a holistic understanding of the sequential electronic response when tracking the development of in-plane and out-of-plane spin correlations. Due to the anisotropy in the in-plane and out-of-plane exchange couplings, the in-plane correlation length exceeds that of the lattice constant at a temperature roughly twice that of T_C , while the out-of-plane spin correlation length reaches that of a lattice constant much closer to T_C , affecting more significantly the Te p orbitals through the Cr-Te-Cr superexchange interactions near T_C . Our results provide a consistent understanding of the two-step evolution of the electronic response to the interplay between local moments in 2D magnets, and demonstrate the sensitivity of using orbital-dependent electronic structure to track evolution of spin correlations in these vdW magnets.

$\text{Cr}_2\text{Ge}_2\text{Te}_6$ forms in the space group 148 ($\bar{R}3$) in a layered structure with weak vdW coupling between adjacent layers [Fig. 1(a)]. The lattice parameters at 15 K determined from neutron scattering are $a = 6.832 \text{ \AA}$ and $c = 20.386 \text{ \AA}$, consistent with previous reports [18,23,39]. The magnetic anisotropy favors the easy axis to be along the c direction. As shown in Fig. 1(b), our field-cooled magnetization measurements show a clear paramagnetic (PM) to FM order transition at 65 K, in agreement with previous studies [18,23,31,32]. In addition, the PM to FM transition can also be clearly observed

in our dilatometry measurement of the c -axis thermal expansion coefficient, α [Fig. 1(b)].

Next, we present the ARPES measured electronic structure in the FM phase. The electronic structure of $\text{Cr}_2\text{Ge}_2\text{Te}_6$ mimics that of a semiconductor, with holelike bands at the Γ points of the Brillouin zone as the valence band top (VBT), consistent with previous reports [18]. We reference the energy axis to the VBT. From the series of constant energy contours, the electronic structure of the valence bands can be seen to evolve from pointlike features at Γ to enlarged pockets at deeper binding energy [Fig. 1(c)]. This is corroborated by dispersions measured along the Γ - M - K - Γ direction. Along this high-symmetry direction, a series of highly dispersive valence bands are centered at the Γ point and merge into relatively flat dispersions in the energy range between -1.0 and -1.5 eV. From comparison to orbital-projected DFT calculations, the highly dispersive bands near the VBT in the FM state are dominated by the Te $5p$ orbital [Fig. 1(f)], while the Cr $3d$ orbitals are mostly concentrated within the energy range between -1.0 and -1.5 eV [40]. The overall electronic structure below T_C as shown in Fig. 1(d) is in qualitative agreement with the DFT calculations [Figs. 1(e) and 1(f)].

To pave the way for understanding the temperature-induced evolution of the electronic structure, we present temperature-dependent ARPES data in Fig. 2. From dispersions along the high-symmetry Γ - M - Γ direction measured at 45 and 200 K, we observe that the insulating nature is persistent across T_C [Figs. 2(a)–2(d)], namely that an electronic gap remains [see Supplemental Material (SM) for gap size discussion [41]]. This is in disagreement with the nonmagnetic DFT calculation [Fig. 1(g)], which predicts a metallic state. As the Cr t_{2g} states are partially filled, this inconsistency suggests that local moments likely survive well above T_C into the paramagnetic phase, driving the system into a Mott insulating state, consistent with the previous report on its sister

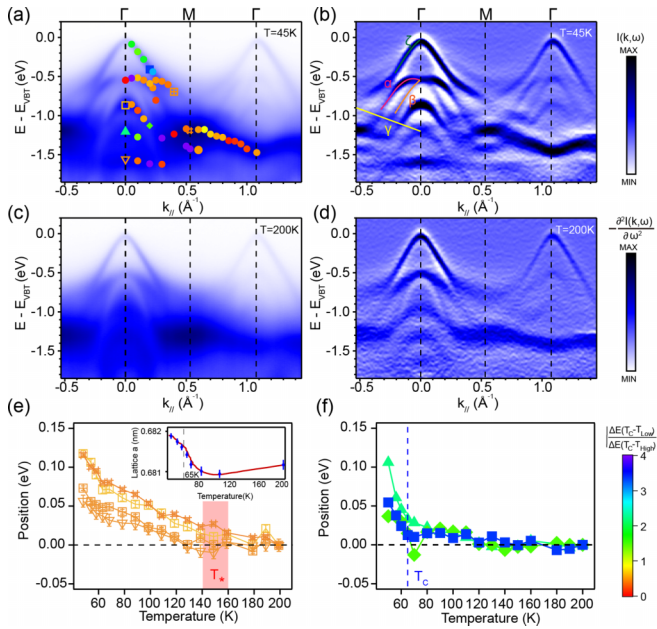


FIG. 2. Temperature evolution and analysis. (a) Raw spectral image and (b) its second energy derivative along Γ - M - Γ measured at 45 K ($T < T_C = 65$ K). (c), (d) Same as (a) and (b) but measured at 200 K. (e), (f) Fitted band position as a function of temperature taken at energy/momentum points as labeled by unique markers in (a). The color of each fitted marker represents the abruptness of change at T_C , defined as $|\frac{\Delta E_{T_C} - T_{low}}{\Delta E_{T_C} - T_{high}}|$. All fitted points are shown in (a), while those with a temperature onset (T_*) well above T_C are shown in (e) and those with changes at T_C are shown in (f). The inset in (e) shows the lattice a as a function of temperature adapted from Ref. [42]. The blue and red lines in (e) and (f) mark the two different temperature scales.

compound $\text{Cr}_2\text{Si}_2\text{Te}_6$ [34]. There are, nevertheless, observable changes across the temperature range. The curvature of the α and β band tops, marked in pink and orange in Fig. 2(b), changes with temperature. In addition, the linearlike band, labeled as γ , disappears with temperature. Besides the overall changes of the α , β , and γ bands, all bands shift with temperature. To better understand the evolution of the bands, we perform a detailed analysis of the energy distribution curves across the Γ - M - Γ cut by fitting and tracking the location of the observable bands (see ARPES Measurements section and Figs. S1–S3 in SM for more details [41]). All fitted bands and momentum points are labeled by unique markers in Fig. 2(a). Interestingly, for all the fittable bands, we can identify two temperature scales where shifts in the band position onset, one at T_C and the other (T_*) around 150 K. To better visualize each band's tendency to shift at the two onset temperatures, we take the ratio of the band shift between T_C and 200 K and between 50 K and T_C , $|\frac{\Delta E_{T_C} - T_{low}}{\Delta E_{T_C} - T_{high}}|$, as the color scale for each marker on each point. A larger value indicates a greater change of the band position at T_C while a value smaller than 1 indicates a larger change at the higher temperature scale T_* . As a result, the changes that are strongly correlated with T_C have a cold color on this scale reflecting a value above 2, and changes correlated with the higher temperature scale will have a warm color reflecting a value below 1. Interestingly, most bands shift

gradually across T_C except those near the VBT marked by green lines named the ζ band in Fig. 1(b), where the changes occur primarily near T_C . This is strongly correlated with the orbital character of the bands, with those primarily associated with Cr $3d$ smoothly evolving across T_C and those with Te $5p$ shifting abruptly across T_C . To better demonstrate this distinct temperature behavior, we plot the temperature-dependent shift for those with an onset primarily at T_* in Fig. 2(e), and those with only an onset primarily at T_C in Fig. 2(f), all referenced to the final band position at 200 K. The dichotomy of the temperature behaviors is clearly contrasted.

As there are no known phase transitions above T_C , the high temperature scale in the band evolution is likely associated with the response of the electronic structure to fluctuation effects associated with the FM order. In $\text{Cr}_2\text{Ge}_2\text{Te}_6$, it has been reported that the lattice parameter a [inset in Fig. 2(e)] shows a negative thermal expansion with an onset temperature near 100 K, well above T_C [42]. To investigate the direct impact of a temperature-dependent lattice change on the electronic structure, we performed DFT calculations using the temperature-dependent lattice parameters refined at 5, 70, and 150 K by neutron scattering experiment [43] (see Fig. S6 in SM for additional neutron scattering data [41]). However, both the direction and magnitude of band shifts are not consistent with the observed band shifts, suggesting that the changes in the electronic structure, particularly those that set in at high temperatures, cannot be directly accounted for by the temperature-induced lattice change.

To gain insights into the possible origin of the higher temperature band evolution, we consider that for a quasi-2D magnet, while the in-plane and out-of-plane spin correlations both diverge at the same rate near T_C , the in-plane correlations, due to larger in-plane exchange interactions, would exceed several lattice constants at higher temperatures compared to those of the out-of-plane correlations, manifesting in a 2D to 3D crossover behavior, as has been reported for the iron-based superconductors [44–46]. In order to investigate this behavior, we probed the magnetic correlations by neutron scattering. First, we observe no broadening of the (110) nuclear and magnetic elastic peaks around T_C [Fig. 3(c)]. Second, we performed a two-axis experiment at $(H, K, L) = (1, 1, 3.43)$. The wave-vector-dependent magnetic susceptibility is proportional to the signal integrated over the energy transfer $E = \frac{k_i^2 - k_f^2}{2m_n}$, with m_n being the mass of neutron [47]. This integration is achieved with a triple-axis spectrometer by removing the analyzer to accept all neutrons along the final wave vector k_f , which was set $\parallel c$. If the magnetic fluctuation is 2D in the ab plane, the magnetic scattering forms a ridge along the $[11L]$ direction. Only at a particular L value, 3.43 in this case, can the condition for the integration over the magnetic ridge be met. Therefore, the two-axis experiment can probe instantaneous spin correlations. No critical 2D divergence in the instantaneous correlations is observed at this wave vector across T_C , as expected since ultimately this is a 3D phase transition [Fig. 3(d)]. Interestingly, previous experiments report a set of critical exponents consistent with those near a 3D tricritical point—a second order to first order crossover point [48–50]. To further determine the temperature-dependent spin excitations across T_C , we performed inelastic neutron

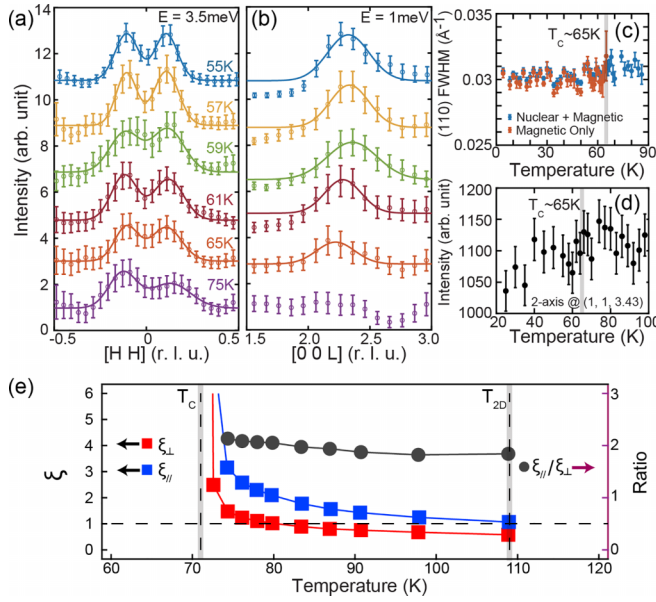


FIG. 3. Neutron scattering and Monte Carlo simulations. (a), (b) Magnetic excitations measured via inelastic neutron scattering along $[HH0]$ and $[00L]$ as a function of temperatures across T_C ; the solid lines are Gaussian fits. (c) The elastic peak width of the (110) peak measured by neutrons. (d) The two-axis measurement at wave vector $(1, 1, 3.43)$. (e) The simulated change in the in-plane ξ_{\parallel} and out-of-plane ξ_{\perp} correlation lengths, in units of the nearest-neighbor lattice spacing, as well as their ratio, as a function of temperature. The crossover scale $T_{2D} \approx 2T_C$ when $\xi_{\parallel} = 1$. The horizontal dotted line is a guide to the eye denoting the nearest-neighbor spacing with T_{2D} indicated here as the point where ξ_{\parallel} begins to exceed this distance.

scattering experiments [51,52], where we measured the spin excitation spectrum at different temperatures around T_C . From Fig. 3(a) we see that the in-plane spin excitations do not vanish up to 75 K and independent measurements show that in-plane spin excitations persist up to at least 150 K (see Fig. S4 and more discussion about temperature dependence of the neutron scattering data in SM [41]), indicating the existence of short-range spin-spin correlations above T_C . For comparison, we measured the out-of-plane spin excitations [Fig. 3(b)], which show a diffusive pattern instead of well-defined spin excitations at 75 K, confirming that the out-of-plane spin correlation length drops below a lattice constant at temperatures slightly above T_C while the in-plane short-range order persists to temperatures well above T_C . This behavior is consistent with the expected development of spin correlations in quasi-2D magnets.

To substantiate this understanding, we carried out classical Monte Carlo simulations using a classical Heisenberg model with the anisotropic exchange couplings from previous reports [5,53,54]. As shown in Fig. 3(e), while both the in-plane correlation length ξ_{\parallel} and the out-of-plane correlation length ξ_{\perp} diverge at T_C , where the ratio of $\xi_{\parallel}/\xi_{\perp}$ is constant, ξ_{\parallel} grows beyond the nearest-neighbor spacing ($\xi > 1$) at a temperature scale (T_{2D}) much higher than that for the out-of-plane correlation. Note that the T_{2D} is not identical to T_* ; T_* is experimentally determined and arises from the anisotropy of

the in-plane and out-of-plane exchange coupling. Hence we can understand that in the range $T_C < T < T_{2D}$, 2D regions of short-range correlated magnetic moments begin to form in plane while the different planes essentially remain uncorrelated, sustaining in-plane spin waves. The electronic structure responds in turn by the shift of Cr d -dominated bands. Just above T_C , out-of-plane correlation length reaches the lattice constant, leading to rapid response in Te p -dominated bands.

With this understanding, we finally discuss the implications for the sequential band evolution observed by ARPES in comparison to DFT calculations. To model the development of in-plane and out-of-plane spin correlations, we model the highest temperature phase above T_{2D} with all single spins antialigned, which effectively mimics the persistence of local moments with no ferromagnetic spin correlations. For $T_{2D} > T > T_C$, we simulate the in-plane FM spin correlations via A-type AFM spin arrangement, where in-plane spins are coaligned. The lowest temperature $T < T_C$ is the FM order where all spins are aligned along the c direction. The orbital projected DFT calculations for these three different models are plotted on top of the corresponding ARPES data (Fig. 4). For the lowest temperature phase ($T < T_C$), the diplike shape for the α and β band top and the linear γ branch in ARPES data are all reproduced by the DFT calculations [Figs. 4(b) and 4(e)]. As the temperature rises above T_C ($T_{2D} > T > T_C$), the α and β band tops evolve into two holelike bands centered at Γ . The β branch with a larger slope and higher energy band top crosses the other branch, consistent with the DFT calculations. When the temperature goes up to 200 K ($T > T_{2D}$), the γ band disappears, again consistent with the disappearance of this feature in the DFT model. As shown in Figs. 4(b)–4(d), besides the great changes in the α , β , and γ bands, the ζ band owns a smaller slope below T_C and evolves into a larger slope dispersion around T_C and exhibits no further dramatic changes above T_C . The ζ band's slope is also well captured by the Te p orbital projected DFT calculations (yellow lines from DFT), suggesting the accuracy of the abstract model. The consistency between the DFT calculations for the three models and the measured temperature evolution of the band dispersions indirectly confirms our understanding that the band evolution manifests the response of the electronic band structure to the sequential development of spin correlations from 2D to 3D.

Overall, supported by our combination of ARPES, neutron scattering, DFT calculations, and Monte Carlo simulations, we come to a comprehensive understanding of the development of the FM order in $\text{Cr}_2\text{Ge}_2\text{Te}_6$. Local moments from Cr d orbitals appear at very high temperatures, resulting in an electronically gapped system. Due to the much larger exchange coupling in the in-plane direction, the correlation length in the in-plane direction exceeds that of a characteristic length scale first, causing bands with predominantly Cr $3d$ character to start evolving well above T_C . With further lowering of the temperature, the out-of-plane correlation length reaches the characteristic length scale near T_C , and is manifested most strongly in the bands associated with Te p orbitals, which play a critical role in bridging the magnetism along the c direction via the Cr-Te-Cr superexchange interactions. The development of spin correlations is typically probed by neutron scattering, which is limited to bulk crystals and not applicable for exfoliated vdW flakes. As a vdW system with

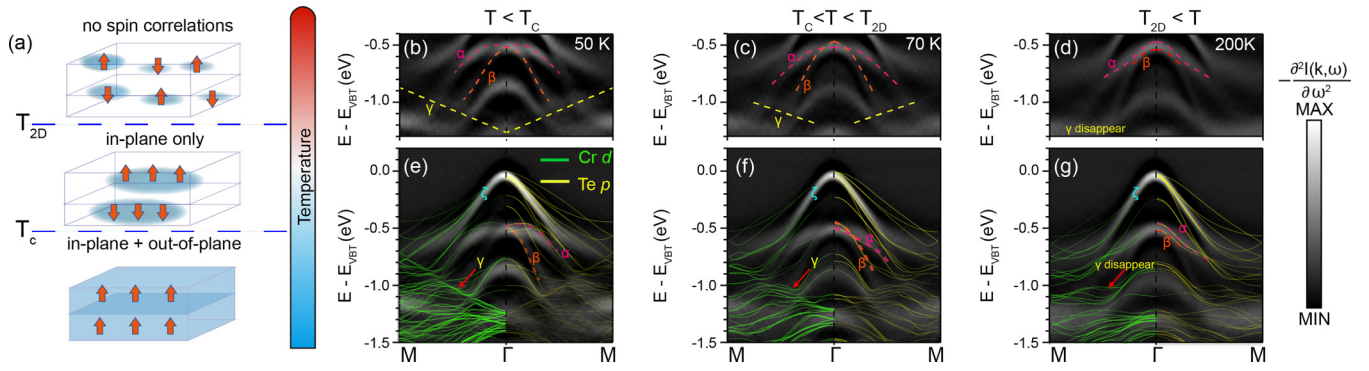


FIG. 4. Spin correlation model and DFT calculations. (a) Schematic for the temperature evolution of spin correlations. Starting with no spin correlations at high temperatures, the in-plane correlations length exceeds the lattice constant first, followed by out-of-plane correlations length, leading to long range FM order at T_c . (b)–(d) Second energy derivatives of ARPES spectra from the three temperature regimes, with eye guides for dominant spectral change. (e)–(g) Same spectra images with corresponding DFT calculations for FM, A-type AFM, and G-type AFM to simulate the three regimes, respectively. The green and yellow lines represent the band structures contributed by Cr 3d and Te 5p projected orbitals, respectively.

a single untangled magnetic order, $\text{Cr}_2\text{Ge}_2\text{Te}_6$ allows us to clearly demonstrate the sensitivity of using orbital-dependent electronic structure to track and resolve the development of spin correlations through the dimensional crossover of the magnetic order in quasi-2D magnets. We anticipate that this sensitivity can be potentially useful in probing the development of spin correlations in the few layer or even monolayer regime, and contribute to the understanding of low dimensional magnetism in the wider class of vdW magnets with more complex order parameters.

ACKNOWLEDGMENTS

This research used resources of the Advanced Light Source, and the Stanford Synchrotron Radiation Lightsources, both U.S. Department Of Energy (DOE) Office of Science User Facilities under Grants No. DE-AC02-05CH11231 and No. AC02-76SF00515, respectively. ARPES work at Rice is supported by DOE Grant No. DE-SC0021421, the Gordon and Betty Moore Foundation’s EPIQS Initiative through Grant No. GBMF9470, and the Robert A. Welch Foundation Grant

No. C-2175 (M.Y.). The neutron scattering and single crystal synthesis work at Rice was supported by NSF Grant No. DMR-2100741 and by the Robert A. Welch Foundation under Grant No. C-1839, respectively (P.D.). Work at University of California, Berkeley, is funded by the U.S. Department of Energy, Office of Science, Office of Basic Energy Sciences (BES), Materials Sciences and Engineering Division under Grant No. DE-AC02-05-CH11231 (Quantum Materials Program No. KC2202). Work at Los Alamos was carried out under the auspices of the DOE National Nuclear Security Administration under Grant No. 89233218CNA000001, and was supported by LANL LDRD Program and in part by Center for Integrated Nanotechnologies, a DOE BES user facility, in partnership with the LANL Institutional Computing Program for computational resources. A portion of this research used resources at the High Flux Isotope Reactor and Spallation Neutron Source, a DOE Office of Science User Facility operated by the Oak Ridge National Laboratory. M.W.B. was funded by the Robert A. Welch Foundation Grant No. C-1818. A.H.N. acknowledges the support of NSF Grant No. DMR-1917511.

- [1] R. J. Birgeneau, The Richtmyer memorial lecture (January 1989): Novel magnetic phenomena and high-temperature superconductivity in lamellar copper oxides, *Am. J. Phys.* **58**, 28 (1990).
- [2] K. S. Burch, D. Mandrus, and J.-G. Park, Magnetism in two-dimensional van der Waals materials, *Nature (London)* **563**, 47 (2018).
- [3] A. H. Castro Neto, F. Guinea, N. M. R. Peres, K. S. Novoselov, and A. K. Geim, The electronic properties of graphene, *Rev. Mod. Phys.* **81**, 109 (2009).
- [4] C. Gong and X. Zhang, Two-dimensional magnetic crystals and emergent heterostructure devices, *Science* **363**, eaav4450 (2019).
- [5] C. Gong, L. Li, Z. Li, H. Ji, A. Stern, Y. Xia, T. Cao, W. Bao, C. Wang, Y. Wang, Z. Q. Qiu, R. J. Cava, S. G. Louie, J. Xia,

and X. Zhang, Discovery of intrinsic ferromagnetism in two-dimensional van der Waals crystals, *Nature (London)* **546**, 265 (2017).

- [6] B. Huang, G. Clark, E. Navarro-Moratalla, D. R. Klein, R. Cheng, K. L. Seyler, D. Zhong, E. Schmidgall, M. A. McGuire, D. H. Cobden, W. Yao, D. Xiao, P. Jarillo-Herrero, and X. Xu, Layer-dependent ferromagnetism in a van der Waals crystal down to the monolayer limit, *Nature (London)* **546**, 270 (2017).
- [7] P. Huang, P. Zhang, S. Xu, H. Wang, X. Zhang, and H. Zhang, Recent advances in two-dimensional ferromagnetism: Materials synthesis, physical properties and device applications, *Nanoscale* **12**, 2309 (2020).
- [8] K. F. Mak, J. Shan, and D. C. Ralph, Probing and controlling magnetic states in 2D layered magnetic materials, *Nat. Rev. Phys.* **1**, 646 (2019).

- [9] Y. Tokura, M. Kawasaki, and N. Nagaosa, Emergent functions of quantum materials, *Nat. Phys.* **13**, 1056 (2017).
- [10] M.-C. Wang, C.-C. Huang, C.-H. Cheung, C.-Y. Chen, S. G. Tan, T.-W. Huang, Y. Zhao, Y. Zhao, G. Wu, Y.-P. Feng, H.-C. Wu, and C.-R. Chang, Prospects and opportunities of 2D van der Waals magnetic systems, *Ann. Phys. (NY)* **532**, 1900452 (2020).
- [11] M. J. Allen, V. C. Tung, and R. B. Kaner, Honeycomb carbon: A review of graphene, *Chem. Rev.* **110**, 132 (2010).
- [12] M. Corasaniti, R. Yang, K. Sen, K. Willa, M. Merz, A. A. Haghhighirad, M. Le Tacon, and L. Degiorgi, Electronic correlations in the van der Waals ferromagnet Fe_3GeTe_2 revealed by its charge dynamics, *Phys. Rev. B* **102**, 161109 (2020).
- [13] M. Corasaniti, R. Yang, Z. Hu, M. Abeykoon, C. Petrovic, and L. Degiorgi, Evidence for correlation effects in noncentrosymmetric type-II Weyl semimetals, *Phys. Rev. B* **104**, L121112 (2021).
- [14] M. Corasaniti, R. Yang, Y. Liu, C. Petrovic, and L. Degiorgi, Optical fingerprints of the electronic band reconstruction in van der Waals magnetic materials, *New J. Phys.* **24**, 123018 (2022).
- [15] S. Ghosh, G. Menichetti, M. I. Katsnelson, and M. Polini, Plasmon-magnon interactions in two-dimensional honeycomb magnets, *Phys. Rev. B* **107**, 195302 (2023).
- [16] J. Huang, Z. Wang, H. Pang, H. Wu, H. Cao, S.-K. Mo, A. Rustagi, A. F. Kemper, M. Wang, M. Yi, and R. J. Birgeneau, Flat-band-induced itinerant ferromagnetism in RbCo_2Se_2 , *Phys. Rev. B* **103**, 165105 (2021).
- [17] W. Jiang, Z. Yang, Y. Li, G. Wang, Q. Jing, D. Guan, J. Ma, W. Zhang, and D. Qian, Spin-split valence bands of the ferromagnetic insulator $\text{Cr}_2\text{Ge}_2\text{Te}_6$ studied by angle-resolved photoemission spectroscopy, *J. Appl. Phys.* **127**, 023901 (2020).
- [18] Y. F. Li, W. Wang, W. Guo, C. Y. Gu, H. Y. Sun, L. He, J. Zhou, Z. B. Gu, Y. F. Nie, and X. Q. Pan, Electronic structure of ferromagnetic semiconductor CrGeTe_3 by angle-resolved photoemission spectroscopy, *Phys. Rev. B* **98**, 125127 (2018).
- [19] G. Menichetti, M. Calandra, and M. Polini, Electronic structure and magnetic properties of few-layer $\text{Cr}_2\text{Ge}_2\text{Te}_6$: The key role of nonlocal electron-electron interaction effects, *2D Mater.* **6**, 045042 (2019).
- [20] G. Menichetti, M. Calandra, and M. Polini, Electrical tuning of the magnetic properties of 2D magnets: The case of $\text{Cr}_2\text{Ge}_2\text{Te}_6$, [arXiv:2312.02887](https://arxiv.org/abs/2312.02887).
- [21] F. Miao, S.-J. Liang, and B. Cheng, Straintronics with van der Waals materials, *Npj Quantum Mater.* **6**, 59 (2021).
- [22] B. Siberchicot, S. Jobic, V. Carreaux, P. Gressier, and G. Ouvrard, Band structure calculations of ferromagnetic chromium tellurides CrSiTe_3 and CrGeTe_3 , *J. Phys. Chem.* **100**, 5863 (1996).
- [23] M. D. Watson, I. Marković, F. Mazzola, A. Rajan, E. A. Morales, D. M. Burn, T. Hesjedal, G. van der Laan, S. Mukherjee, T. K. Kim, C. Bigi, I. Vobornik, M. C. Hatnean, G. Balakrishnan, and P. D. C. King, Direct observation of the energy gain underpinning ferromagnetic superexchange in the electronic structure of CrGeTe_3 , *Phys. Rev. B* **101**, 205125 (2020).
- [24] R. Yang, M. Corasaniti, C. C. Le, C. Yue, Z. Hu, J. P. Hu, C. Petrovic, and L. Degiorgi, Charge dynamics of a noncentrosymmetric magnetic Weyl semimetal, *npj Quantum Mater.* **7**, 101 (2022).
- [25] J. Zhang, X. Cai, W. Xia, A. Liang, J. Huang, C. Wang, L. Yang, H. Yuan, Y. Chen, S. Zhang, Y. Guo, Z. Liu, and G. Li, Unveiling electronic correlation and the ferromagnetic superexchange mechanism in the van der Waals crystal CrSiTe_3 , *Phys. Rev. Lett.* **123**, 047203 (2019).
- [26] J.-X. Zhu, M. Janoschek, D. S. Chaves, J. C. Cezar, T. Durakiewicz, F. Ronning, Y. Sassa, M. Mansson, B. L. Scott, N. Wakeham, E. D. Bauer, and J. D. Thompson, Electronic correlation and magnetism in the ferromagnetic metal Fe_3GeTe_2 , *Phys. Rev. B* **93**, 144404 (2016).
- [27] A. K. Geim and I. V. Grigorieva, Van der Waals heterostructures, *Nature (London)* **499**, 419 (2013).
- [28] B. Liu, Y. Zou, L. Zhang, S. Zhou, Z. Wang, W. Wang, Z. Qu, and Y. Zhang, Critical behavior of the quasi-two-dimensional semiconducting ferromagnet CrSiTe_3 , *Sci. Rep.* **6**, 33873 (2016).
- [29] Y. Liu and C. Petrovic, Critical behavior of quasi-two-dimensional semiconducting ferromagnet $\text{Cr}_2\text{Ge}_2\text{Te}_6$, *Phys. Rev. B* **96**, 054406 (2017).
- [30] A. H. MacDonald, P. Schiffer, and N. Samarth, Ferromagnetic semiconductors: moving beyond (Ga, Mn)As, *Nat. Mater.* **4**, 195 (2005).
- [31] M. Suzuki, B. Gao, K. Koshiishi, S. Nakata, K. Hagiwara, C. Lin, Y. X. Wan, H. Kumigashira, K. Ono, S. Kang, S. Kang, J. Yu, M. Kobayashi, S.-W. Cheong, and A. Fujimori, Coulomb-interaction effect on the two-dimensional electronic structure of the van der Waals ferromagnet $\text{Cr}_2\text{Ge}_2\text{Te}_6$, *Phys. Rev. B* **99**, 161401(R) (2019).
- [32] T. Yilmaz, R. M. Geilhufe, I. Pletikosić, G. W. Fernando, R. J. Cava, T. Valla, E. Vescovo, and B. Sinkovic, Multi-hole bands and quasi-two-dimensionality in $\text{Cr}_2\text{Ge}_2\text{Te}_6$ studied by angle-resolved photoemission spectroscopy, *Europhys. Lett.* **133**, 27002 (2021).
- [33] I. Žutić, J. Fabian, and S. Das Sarma, Spintronics: Fundamentals and applications, *Rev. Mod. Phys.* **76**, 323 (2004).
- [34] T. J. Williams, A. A. Aczel, M. D. Lumsden, S. E. Nagler, M. B. Stone, J.-Q. Yan, and D. Mandrus, Magnetic correlations in the quasi-two-dimensional semiconducting ferromagnet CrSiTe_3 , *Phys. Rev. B* **92**, 144404 (2015).
- [35] A. Ron, E. Zoghlin, L. Balents, S. D. Wilson, and D. Hsieh, Dimensional crossover in a layered ferromagnet detected by spin correlation driven distortions, *Nat. Commun.* **10**, 1654 (2019).
- [36] H. Wu, A. M. Hallas, X. Cai, J. Huang, J. S. Oh, V. Loganathan, A. Weiland, G. T. McCandless, J. Y. Chan, S.-K. Mo, D. Lu, M. Hashimoto, J. Denlinger, R. J. Birgeneau, A. H. Nevidomskyy, G. Li, E. Morosan, and M. Yi, Nonsymmorphic symmetry-protected band crossings in a square-net metal PtPb_4 , *npj Quantum Mater.* **7**, 31 (2022).
- [37] H. Wu, L. Chen, P. Malinowski, J. Huang, Q. Deng, K. Scott, B. G. Jang, J. P. C. Ruff, Y. He, X. Chen, C. Hu, Z. Yue, J. S. Oh, X. Teng, Y. Guo, M. Klemm, C. Shi, Y. Shi, C. Setty, T. Werner *et al.*, Reversible non-volatile electronic switching in a near room temperature van der waals ferromagnet, [arXiv:2307.03154](https://arxiv.org/abs/2307.03154).
- [38] H. Wu, C. Hu, Y. Xie, B. G. Jang, J. Huang, Y. Guo, S. Wu, C. Hu, Z. Yue, Y. Shi, Z. Ren, T. Yilmaz, E. Vescovo, C. Jozwiak, A. Bostwick, E. Rotenberg, A. Fedorov, J. Denlinger, C. Klewe, P. Shafer *et al.*, Spectral evidence for local-moment

- ferromagnetism in van der Waals metals Fe_3GaTe_2 and Fe_3GeTe_2 , [arXiv:2307.00441](https://arxiv.org/abs/2307.00441).
- [39] D.-Y. Wang, Q. Jiang, W.-J. Liu, H.-J. Qian, H.-M. Zha, Z.-C. Jiang, S. Qiao, and M. Ye, In-plane momentum-dependent spin texture originating from surface symmetry breaking in the two-dimensional van der Waals ferromagnet CrGeTe_3 , *Phys. Rev. B* **107**, 125148 (2023).
- [40] P. Blaha, K. Schwarz, G. K. H. Madsen, D. Kvasnicka, J. Luitz, R. Laskowski, F. Tran, L. Marks, and L. Marks, *WIEN2k: An Augmented Plane Wave Plus Local Orbitals Program for Calculating Crystal Properties*, Technische Universität, 2019.
- [41] See Supplemental Material at <http://link.aps.org/supplemental/10.1103/PhysRevB.109.045416> for the detailed temperature-dependent electronic structure, examples of the fitting process, additional fitted band evolution, inelastic neutron scattering data at 55 and 150 K, lattice induced band change from DFT, orbital projected DFT calculations, and the photon energy dependent band structure. The Supplemental Material also contains Refs. [5,40,48,49,51–53].
- [42] V. Cartheaux, D. Brunet, G. Ouvrard, and G. Andre, Crystallographic, magnetic and electronic structures of a new layered ferromagnetic compound $\text{Cr}_2\text{Ge}_2\text{Te}_6$, *J. Phys.: Condens. Matter* **7**, 69 (1995).
- [43] J. Huang, S. Li, C. Yoon, J. S. Oh, H. Wu, X. Liu, N. Dhale, Y.-F. Zhou, Y. Guo, Y. Zhang, M. Hashimoto, D. Lu, J. Denlinger, X. Wang, C. N. Lau, R. J. Birgeneau, F. Zhang, B. Lv, and M. Yi, Room-temperature topological phase transition in quasi-one-dimensional material Bi_4I_4 , *Phys. Rev. X* **11**, 031042 (2021).
- [44] J. Huang, R. Yu, Z. Xu, J.-X. Zhu, J. S. Oh, Q. Jiang, M. Wang, H. Wu, T. Chen, J. D. Denlinger, S.-K. Mo, M. Hashimoto, M. Michiardi, T. M. Pedersen, S. Gorovikov, S. Zhdanovich, A. Damascelli, G. Gu, P. Dai, J.-H. Chu, D. Lu, Q. Si, R. J. Birgeneau, and M. Yi, Correlation-driven electronic reconstruction in $\text{FeTe}_{1-x}\text{Se}_x$, *Commun. Phys.* **5**, 29 (2022).
- [45] S. D. Wilson, Z. Yamani, C. R. Rotundu, B. Freelon, P. N. Valdivia, E. Bourret-Courchesne, J. W. Lynn, S. Chi, T. Hong, and R. J. Birgeneau, Antiferromagnetic critical fluctuations in BaFe_2As_2 , *Phys. Rev. B* **82**, 144502 (2010).
- [46] M. Yi, H. Pfau, Y. Zhang, Y. He, H. Wu, T. Chen, Z. R. Ye, M. Hashimoto, R. Yu, Q. Si, D.-H. Lee, P. Dai, Z.-X. Shen, D. H. Lu, and R. J. Birgeneau, Nematic energy scale and the missing electron pocket in FeSe , *Phys. Rev. X* **9**, 041049 (2019).
- [47] L. Chen, J.-H. Chung, T. Chen, C. Duan, A. Schneidewind, I. Radelytskyi, D. J. Voneshen, R. A. Ewings, M. B. Stone, A. I. Kolesnikov, B. Winn, S. Chi, R. A. Mole, D. H. Yu, B. Gao, and P. Dai, Magnetic anisotropy in ferromagnetic CrI_3 , *Phys. Rev. B* **101**, 134418 (2020).
- [48] L. Chen, C. Mao, J.-H. Chung, M. B. Stone, A. I. Kolesnikov, X. Wang, N. Murai, B. Gao, O. Delaire, and P. Dai, Anisotropic magnon damping by zero-temperature quantum fluctuations in ferromagnetic CrGeTe_3 , *Nat. Commun.* **13**, 4037 (2022).
- [49] M. E. Fisher, The theory of equilibrium critical phenomena, *Rep. Prog. Phys.* **30**, 615 (1967).
- [50] G. T. Lin, H. L. Zhuang, X. Luo, B. J. Liu, F. C. Chen, J. Yan, Y. Sun, J. Zhou, W. J. Lu, P. Tong, Z. G. Sheng, Z. Qu, W. H. Song, X. B. Zhu, and Y. P. Sun, Tricritical behavior of the two-dimensional intrinsically ferromagnetic semiconductor CrGeTe_3 , *Phys. Rev. B* **95**, 245212 (2017).
- [51] G. E. Granroth, A. I. Kolesnikov, T. E. Sherline, J. P. Clancy, K. A. Ross, J. P. C. Ruff, B. D. Gaulin, and S. E. Nagler, SEQUOIA: A newly operating chopper spectrometer at the SNS, *J. Phys.: Conf. Ser.* **251**, 012058 (2010).
- [52] M. B. Stone, J. L. Niedziela, D. L. Abernathy, L. DeBeer-Schmitt, G. Ehlers, O. Garlea, G. E. Granroth, M. Graves-Brook, A. I. Kolesnikov, A. Podlesnyak, and B. Winn, A comparison of four direct geometry time-of-flight spectrometers at the spallation neutron source, *Rev. Sci. Instrum.* **85**, 045113 (2014).
- [53] S. G. Pawig and K. Pinn, Monte carlo algorithms for the fully frustrated XY model, *Int. J. Mod. Phys. C* **09**, 727 (1998).
- [54] U. Wolff, Collective Monte Carlo updating for spin systems, *Phys. Rev. Lett.* **62**, 361 (1989).